Journal of Molecular Structure 1049 (2013) 303–309

Contents lists available at SciVerse ScienceDirect

Journal of Molecular Structure

journal homepage: www.elsevier.com/locate/molstruc

Investigation of the azo-hydrazone tautomeric equilibrium in an azo dye involving the naphthalene moiety by UV–vis spectroscopy and quantum chemistry

Arslan Ünal [a,*], Bilge Eren [b], Erdal Eren [b]

[a] Department of Physics, Science and Arts Faculty Bilecik Şeyh Edebali University, 11210 Bilecik, Turkey
[b] Department of Chemistry, Science and Arts Faculty Bilecik Şeyh Edebali University, 11210 Bilecik, Turkey

HIGHLIGHTS

- EBB exhibited the acid–base, azo-hydrazone and aggregate equilibria in DMF solution.
- EBB mainly existed in the azo form in MeCN solution.
- In MeCN solution, the main absorption band of dye showed a hypsochromic shift with time.
- In DMF solution, the main absorption band of dye showed a bathochromic shift with time.
- Observed changes with increasing temperature are reversible in DMF solution.

GRAPHICAL ABSTRACT

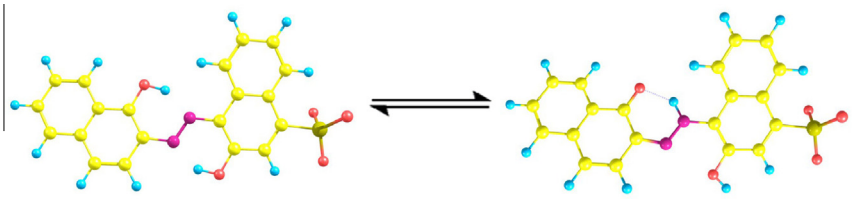

The azo-hydrazone equilibrium of EBB.

ARTICLE INFO

Article history:
Received 15 January 2013
Received in revised form 14 June 2013
Accepted 16 June 2013
Available online 1 July 2013

Keywords:
Azo dye
UV–vis spectra
Azo-hydrazone tautomerism
Aggregation
Solvent effect
DFT

ABSTRACT

Photophysical properties of the azo-hydrazone tautomerism of Eriochrome Blue Black B (1-(1-hydroxy-2-naphthylazo)-2-naphthol-4-sulphonic acid) in DMF, MeCN and water were investigated using UV–visible spectroscopy and quantum chemical calculations. The optimized molecular structure parameters, relative energies, mole fractions, electronic absorption spectra and HOMO–LUMO energies for possible stable tautomeric forms of EBB were theoretically calculated by using hybrid density functional theory, (B3LYP) methods with 6-31G(d) basis set level and polarizable continuum model (PCM) for solvation effect. The effects of varying pH-, dye concentration-, solvent-, temperature-, and time-dependences on the UV–vis spectra of Eriochrome Blue Black B were also investigated experimentally. The calculations showed that the dye exhibited acid–base, azo-hydrazone and aggregate equilibria in DMF solution, while the most probably preferred form in MeCN solution was azo form. Thermodynamic parameters of dimerization reaction in DMF solution proved that entropy was the driving force of this reaction.

1. Introduction

The azo compounds are among the largest group of dyes with over one thousand compounds being commercially offered. These dyes show considerable activity in high-tech applications especially in the electronics and nonimpact printing industries. They are also extensively used for dyeing fabrics and coloring agents in inks. In last two decades, there is a rapidly growing interest in the potential of their biochemical applications [1–3] and in their use for optical data storage [4–7]. The applications of these dyes are strongly depended on their photophysical properties. For instance, photophysical properties of azo-hydrazone tautomerism have been used to some extent for dye location characterization in surfactant micelles and textile fibers [8–10], photographic systems [11], dyeing [12], bleaching [13–15] and polymers [16,17].

* Corresponding author. Tel.: +90 228 216 1479; fax: +90 228 216 0080.
E-mail address: arslan.unal@bilecik.edu.tr (A. Ünal).

0022-2860/$ - see front matter © 2013 Elsevier B.V. All rights reserved.
http://dx.doi.org/10.1016/j.molstruc.2013.06.037

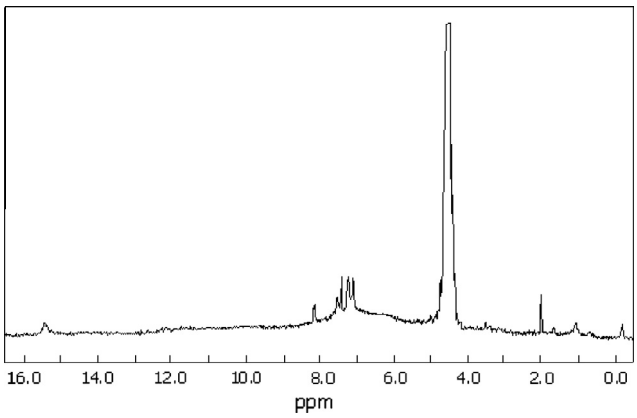

Fig. 1. ^{1}H NMR spectrum of EBB in D_2O.

The Eriochrome Blue Black (EBB) azo dyes have attracted special interest in various applications as well, such as metal chelates for dyeing protein [18], chromogenic indicator [19], and dye location characterization in surfactant micelles [20] and probe molecules to characterize catalysts [21,22].

The characterization and the understanding of tautomerization mechanism are crucial for controlling the molecular properties depending on the polarity and pH of the medium. In view of the above observations, we thought it is worthwhile to study the spectral behavior of an azo dye involving the naphthalene moiety in pure and series of mixed organic solvents in various polarities. In this study, we focused on the objective to assess the impact of the effects of pH-, dye concentration-, solvent-, temperature-, and time-dependences on the UV–vis. spectra of Eriochrome Blue Black B (EBB) azo dye. In addition, some electronic structure properties of tautomeric forms were investigated by using DFT quantum chemical calculations in order to give more insight into the azo-hydrazone tautomerism and to confirm the experimental findings.

2. Experimental

2.1. Materials

EBB was purchased from Aldrich and used without additional purification. Dimethylformamide (DMF) and acetonitrile (MeCN) were of analytical grade (Merck). Boric acid, phosphoric acid, acetic acid and sodium hydroxide for Britton Robinson (BR) buffer were obtained from Merck product. BR buffer solution was prepared as follows: 0.05 M acetic acid, 0.05 M phosphoric acid and 0.05 M boric acid solutions were prepared separately in 100 mL volumetric flasks and then the solutions were mixed together with requisite volume for buffer solution. Solutions (8×10^{-2} M) of EBB were prepared by dissolving the accurately weighed amount of the target compound in the required amount of the appropriate solvent. Solutions of lower concentrations for the spectral measurements were prepared by dilution.

2.2. Methodology

The electronic absorption spectra of 8.0×10^{-4} M of EBB solution were recorded in BR buffer in the presence of 0.1 M KCl using with different pH ranging from 1.6 to 12.3. The pH values were checked by using a Jenway 3040 Model digital pH-meter. The water was used as ultra pure water by passing deionized water through a Milli-Q water purification system. The electronic spectra were recorded on a Unicam-2 UV–vis spectrophotometer at 22 ± 1.0 °C by using 1 cm matched quartz cells. The examination of temperature effect was searched by using GBC Cintra20 UV–vis spectrophotometer combined with a cell temperature controller with ±0.1 °C accuracy. The ^{1}H NMR spectrum was recorded on a Bruker AC 200 Fourier Transform Spectrometer operating at 200 MHz in D_2O.

3. Theoretical

All theoretical calculations were performed by using Gaussian 03W program package [23]. The equilibrium molecular geometries for three possible tautomers of EBB (one azo and two hydrazone forms) were considered for geometry optimization by using the density functional theory (DFT) method by Becke's three-parameter exchange functional and gradient-corrected functional of Lee, Yang and Parr (B3LYP) hybrid functional at 6-31G(d) basis set level [24,25]. The solution phase geometry optimizations of tautomeric structures were performed at the same theory level as polarizable continuum model (PCM) [26,27]. Dimethylformamide [DMF; $(CH_3)_2NC(=O)H$] was used as a solvent (since DMF is not available in Gaussian03's PCM method, it was defined according to the following parameters [28]: EPS = 36.71, RSOLV = 2.647, and

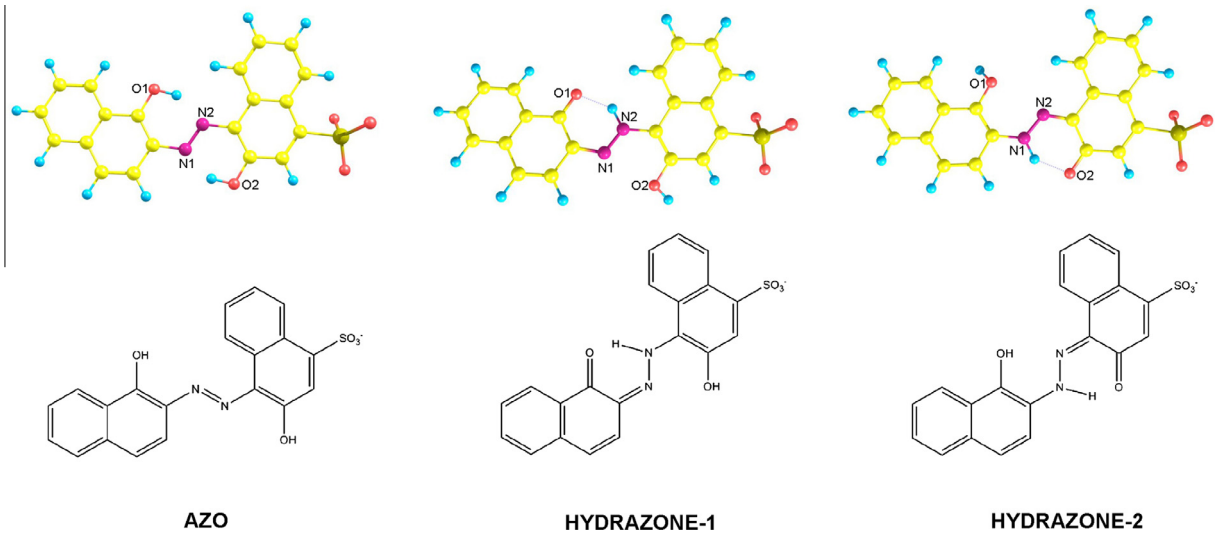

Fig. 2. Illustration for the three stable tautomers of EBB.

DENSITY = 0.00778), and the universal force field (UFF) model was applied to build up the molecular cavity. No symmetry restriction was applied during the geometry optimizations in solvent media and gas phase. The vibrational frequencies of each tautomers were computed at the optimized geometries to ensure that no imaginary frequencies were obtained, confirming that they correspond to true minima on the potential energy surfaces. Gibbs free energy values (ΔG), which were calculated at B3LYP/6-31G(d) within the harmonic approximation, were used for the evaluation of the tautomeric mole fractions [29]. Electronic absorption spectra of the preferred tautomeric forms were predicted by using TD-DFT [30] in the calculation of electronic excitation energies for gas and solution phases. In addition, frontier molecular orbital analysis of azo and hydrazone tautomeric forms were also calculated.

4. Results and discussion

4.1. NMR spectroscopy of EBB in D_2O

The ^{1}H NMR spectrum of EBB in D_2O is shown in Fig. 1. There are a number of NMR lines between 0 and 4 ppm are probably due to impurities, and a highly intense line in ca. 5 ppm is due to water of D_2O. The lines between 7 and 8 ppm also belong to the aromatic ring protons. A relatively broad and less-intense NMR line in the range from 15 to 16 ppm may be related to the proton signal of N—H, and may also be due to the dynamic behavior of hydrogen exchange between EBB molecule and solvent molecules. We could not get precise information about the existence of azo-hydrazone tautomerism from the ^{1}H NMR spectrum of EBB. For this reason, the UV–vis spectroscopy technique was applied to investigate the azo-hydrazone tautomeric equilibrium of EBB.

4.2. Computational results

DFT calculations were performed for the three tautomers of EBB. The optimized molecular structures of azo and two hydrazone tautomers are depicted in Fig. 2. The calculated relative energies in gas and solution phases at room-temperature are also presented in Table 1. The azo tautomer is more stable than the hydrazone-1 and hydrazone-2 tautomers by 8.74 and 14.62 kcal/mol in gas phase. The energy differences in solution media between azo and hydrazone tautomers ranged from 1.70 to 5.46 kcal/mol, as shown in the ΔE_0 row of Table 1. Table 2 shows that hydrogen bond lengths of the hydrazone tautomers were 1.736–1.743 Å, which are in the range of general hydrogen bond length of 1.7 Å. N1—N2 bond lengths in azo and hydrazone tautomers are ca. 1.288 Å, indicating more double bond character, and ca. 1.304 Å, indicating more single bond character, respectively.

The relative stability of three tautomers was also investigated by tautomeric mole fraction according to their calculated ΔG energies. The tautomeric mole fraction calculations show that the azo form is the most stable form of EBB with 100% value in gas phase and more than 90% in solution phase. Besides the mole fraction of hydrazone-1 tautomer becomes in the range from ca. 7% to 10%, while the polarity of solvent increases. On the other hand, hydrazone-2 tautomer has 0% mole fraction in both phases. Due to the relative energy and tautomeric equilibrium results, the azo and hydrazone-1 (hereinafter referred to as hydrazone) tautomeric forms were considered in the UV–vis spectroscopic analysis.

Before offering an explanation for the UV–vis spectra of EBB, the frontier molecular orbitals (FMO) of azo and hydrazone tautomeric forms in DMF are shown in Fig. 3. The HOMO and LUMO of azo and hydrazone tautomeric forms are delocalized over the whole main skeleton of EBB. As expected, all the frontier molecular orbitals show π characters. The energy gap value between HOMO and

Table 1
The selected molecular features for the azo and hydrazone tautomers of EBB at DFT-B3LYP/6-31G(d) level of theory.

	ε = 1			ε = 36.64			ε = 36.71			ε = 78.39		
	Azo	Hydrazone 1	Hydrazone 2	Azo	Hydrazone 1	Hydrazone 2	Azo	Hydrazone 1	Hydrazone 2	Azo	Hydrazone 1	Hydrazone 2
Symmetry	C_1	C_1	C_1	C_1	C_1	C_1	C_1	C_1	C_1	C_1	C_1	C_1
μ (debye)	20.114	18.072	23.596	30.518	27.060	34.503	30.501	27.057	34.472	30.886	27.374	34.950
E_{tot} (kcal/mol)	−1037766.934	−1037758.445	−1037752.313	−1037826.083	−1037823.642	−1037820.192	−1037826.084	−1037823.637	−1037820.188	−1037827.917	−1037825.922	−1037822.693
E_0 (kcal/mol)	−1037580.845	−1037572.108	−1037566.523	−1037640.742	−1037638.596	−1037635.285	−1037640.737	−1037638.589	−1037637.786	−1037642.688	−1037640.989	−1037637.921
ZPVE(kcal/mol)	186.089	186.337	185.790	185.341	185.047	184.908	185.347	185.048	184.908	185.229	184.933	184.773
ΔE_{tot} (kcal/mol)	0.000	8.489	14.621	0.000	2.441	5.891	0.000	2.447	5.896	0.000	1.925	5.224
ΔE_0 (kcal/mol)	0.000	8.737	14.322	0.000	2.146	5.457	0.000	2.148	2.951	0.000	1.699	4.767
ΔG (kcal/mol.)	−1037613.521	−1037605.362	−1037600.113	−1037673.392	−1037671.912	−1037668.874	−1037673.449	−1037671.892	−1037668.975	−1037675.475	−1037674.192	−1037671.602
$\Delta\Delta G$ (kcal/mol.)	0.000	8.159	13.408	0.000	1.480	4.518	0.000	1.557	4.474	0.000	1.283	3.873
Mole fractions (%)	100.00	0.00	0.00	92.42	7.58	0.00	93.28	6.72	0.00	89.69	10.31	0.00
HOMO (eV)	−2.547	−2.535	−2.359	−5.364	−5.240	−5.262	−5.364	−5.241	−5.262	−5.396	−5.281	−5.292
LUMO (eV)	−0.215	−0.142	0.106	−2.618	−2.417	−2.484	−2.618	−2.417	−2.484	−2.648	−2.459	−2.530
ΔH–L (eV)	−2.332	−2.393	−2.465	−2.746	−2.823	−2.778	−2.746	−2.824	−2.778	−2.748	−2.822	−2.762

Table 2
Bond length of the tautomers geometrically optimized with DFT-B3LYP/6-31G(d) level of theory.

Solvent (ε)	Intra-molecular hydrogen bond length (Å)			N1—N2 bond length (Å)		
	Azo	Hydrazone-1 (N2—H...O1)	Hydrazone-2 (N1—H...O2)	Azo (—N1=N2—)	Hydrazone-1 (=N1—N2—)	Hydrazone-2 (—N1—N2=)
Gas (1)	–	1.721	1.697	1.295	1.298	1.324
MeCN (36.64)	–	1.737	1.738	1.288	1.306	1.303
DMF (36.71)	–	1.736	1.737	1.288	1.306	1.303
H_2O (78.39)	–	1.740	1.743	1.287	1.306	1.302

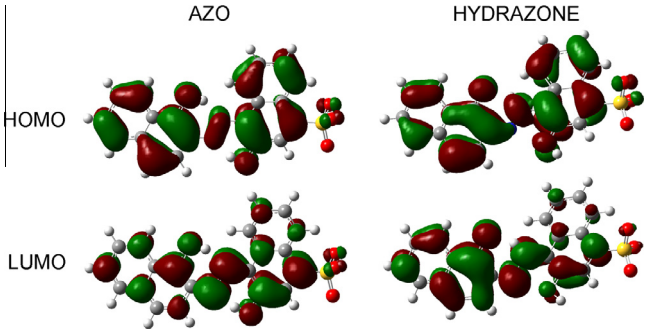

Fig. 3. The molecular orbital surfaces of EBB for azo and hydrazone forms in DMF.

LUMO of both forms is similar and is found to be around −2.4 eV for gas phase and −2.8 eV for solution media. This similarity also shows that the FMO topologies and sizes are similar for the both tautomeric forms of EBB.

4.3. UV–visible spectroscopic study

4.3.1. Preliminary remarks

The first six spin-allowed singlet–singlet excitations for azo and hydrazone forms of EBB were calculated by TD-DFT approach at the same theory level. TD-DFT calculations were started from optimized geometry by using the same level of theory and performed for gas and solution phases to calculate the excitation energies. The percentage distributions of molecular orbitals to formation of the bands were obtained by using SWizard Program [31]. For both forms of EBB, maximum wavelength (λ_{max}), oscillator strength (f), excitation energy (eV) and major contributions of the calculated transitions are given in Table 3. The main absorption band at 490 nm for azo form and the other at 521 nm for hydrazone form arise excitation from HOMO−1 to LUMO transition in gas phase. However, the absorption bands between 500 and 510 nm arise excitations from HOMO to LUMO for the both form of EBB in solution phases. This band must be related to a $\pi \rightarrow \pi^*$ transition contributing the whole electronic system of EBB in conjugation between the two forms of the chromophore.

4.3.2. Effect of pH on the electronic absorption spectra

The electronic absorption spectra of 0.8 mM of EBB solution were recorded in BR buffer in the presence of 0.1 M KCl at different pH values from 1.6 to 12.3 and 0.1 M NaOH (Fig. 4). As shown in Fig. 4, EBB indicated the non-simple ionization step. EBB contains

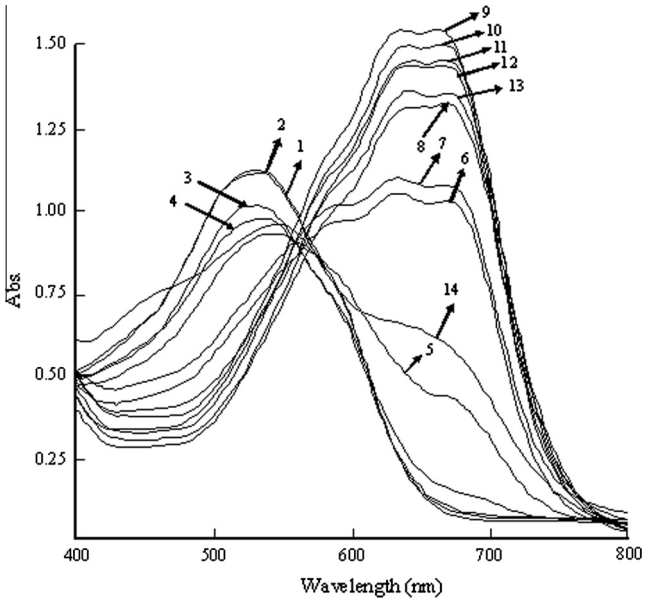

Fig. 4. Electronic absorption spectra of 0.80 mM solution of EBB in BR buffer solutions (1) 1.6; (2) 2.4; (3) 3.6; (4) 4.6; (5) 5.5; (6) 6.3; (7) 6.9; (8) 7.4; (9) 8.2; (10) 9.4; (11) 10.5; (12) 11.3; (13) 12.3; (14) 0.1 M NaOH.

three ionizable protons. The first proton (in the sulfonate group) was very acidic and non-detectable in the pH range. Hence, the existing species in the acidic range up to pH 3.6 was H_2D^- and was also shown by the absorption band with a maximum at 532 nm (Fig. 4). At higher pH values, the visible spectrum of EBB showed a new absorption bands as a shoulder at 598 nm and a splitting band appearing between 640 and 670 nm due to the di-anionic form of EBB. The absorption band maxima at higher wavelengths increased in the pH range from 6.3 to 8.2. On the contrary, these bands decreased in the pH range from 9.4 to 12.3. The increase in the baseline up to 0.08 A at 750–800 nm and distorted isosbestic points with increasing pH indicated the pH-dependent aggregation. This conclusion was also supported by the plot of absorbance vs. pH at 640 nm in pH range 1.6–12.3 has not a sigmoidal form (not shown). This result also proved the aggregation beside the acid–base equilibria. The shoulder band at 598 nm was most probably due to the di-anionic form of monomeric EBB. The red-shifted and overlapped bands comparing to the di-

Table 3
The calculated electronic absorption spectra data for the azo and hydrazone forms of EBB.

Solvent (ε)	TD-DFT-B3LYP/6-31G(d)							
	Azo form				Hydrazone form			
	λ_{max} (nm)	Oscillator strength (f)	Energy (eV)	Major contribution	λ_{max} (nm)	Oscillator strength (f)	Energy (eV)	Major contribution
Gas (1.00)	490.48	0.7689	2.53	H-1 → L (74%)	521.18	0.6373	2.38	H-1 → L (76%)
MeCN (36.64)	509.28	0.7138	2.43	H → L (79%)	501.07	0.6129	2.47	H → L (79%)
DMF (36.71)	508.40	0.7075	2.44	H → L (79%)	500.39	0.6106	2.48	H → L (79%)
H_2O (78.39)	509.24	0.6999	2.43	H → L (79%)	501.22	0.6138	2.47	H → L (79%)

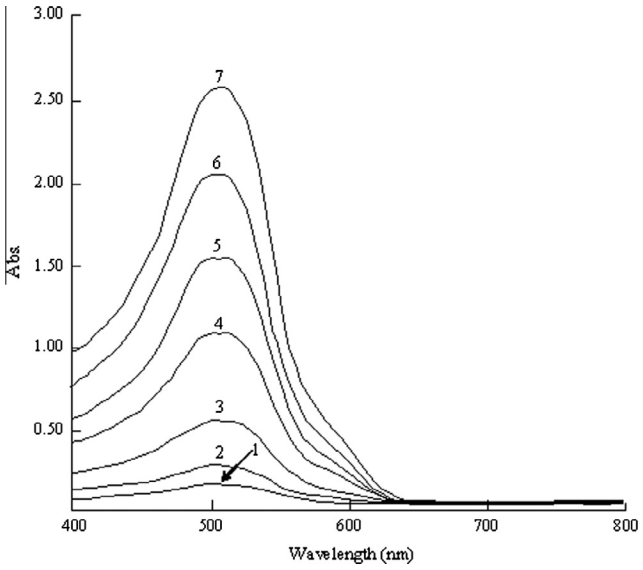

Fig. 5. Electronic absorption spectra of EBB in MeCN; [EBB] mM = 0.05 (1); 0.15 (2); 0.25 (3); 0.45 (4); 0.65 (5); 0.70 (6); 0.85 (7).

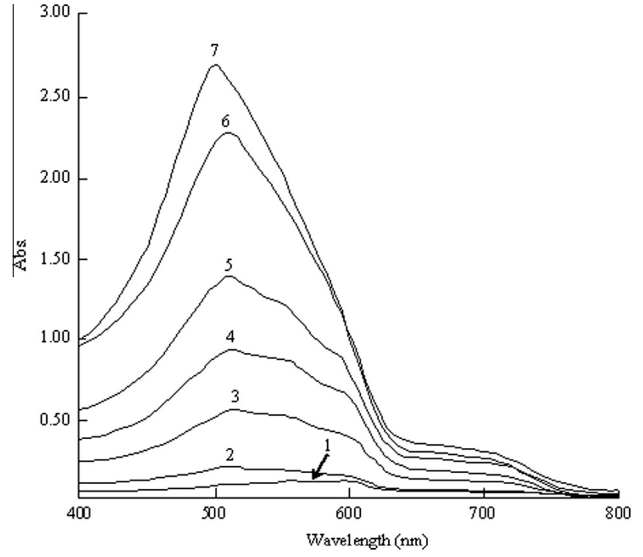

Fig. 6. Electronic absorption spectra of EBB in DMF; [EBB] mM = 0.05 (1); 0.15 (2); 0.35 (3); 0.45 (4); 0.65 (5); 0.85 (6); 1.25 (7).

anionic form demonstrated to the aggregation of di-anionic form of EBB. The splitting of the absorption spectra at longer wavelengths showed the excitonic coupling between transition dipoles on neighboring molecules. In other words, the dipole–dipole interaction between the adjacent molecules in the aggregate splits the electronic transitions into a broad band with different wavelengths. It is related the distance between the interacting centers, and the orientation of the di-anionic monomers with respect to each other [32–34].

The absorption band of the three-anionic form D^{3-} appeared at 540 nm in the presence of 0.1 M NaOH solution. The similarity between the UV–vis. spectra of the three-anionic and mono-anionic form showed that mono-ionized EBB form existed in azo structure. Because, the three-anionic form of EBB is in the azo structure. This result showed that the ionization step from $(H_2D)_2^-$ to the D^{3-}

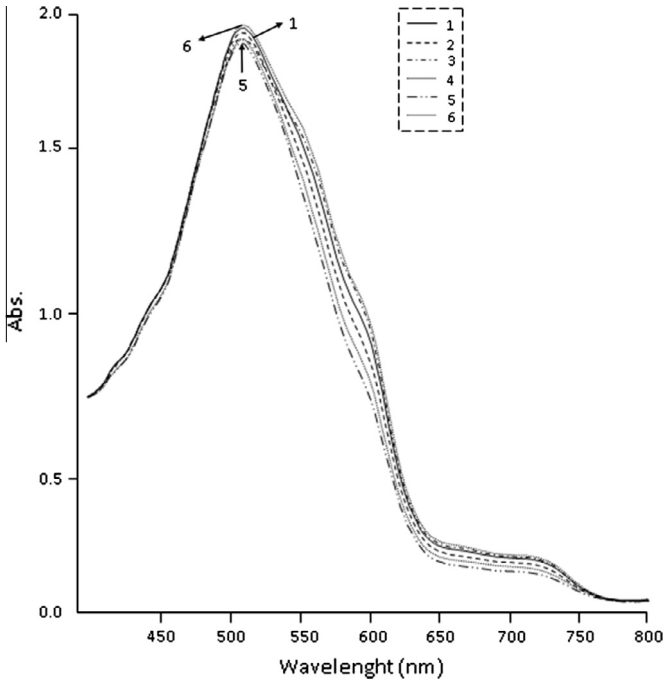

Fig. 7. The temperature effect on the electronic absorption spectra of 0.70 mM EBB in DMF. For each curve is given the measurement temperature in °C. (1) 30; (2) 40; (3) 50; (4) 60; (5) 70; (6) after cooling to room temperature.

passed through the inter-conversion between the different species of EBB.

$$\underset{\lambda=532\pm\Delta\lambda nm}{(H_2D^-)_2} \overset{pH<5.5}{\leftrightarrow} \underset{\lambda=598nm}{HD^{2-}} + 2H^+ \overset{pH<6.9}{\leftrightarrow} \underset{\lambda=640,670nm}{(HD^{2-})_2} \overset{<0.1M\ NaOH}{\leftrightarrow} \times \underset{\lambda=540nm}{D^{3-}} + 2H^+ \quad (1)$$

4.3.3. Solvent and temperature effects on EBB tautomer forms

The visible absorption spectra of EBB at different concentrations were recorded in MeCN and DMF solvents (Figs. 5 and 6). In MeCN solution, one symmetrical visible band at 508 nm was observed mainly in the azo form. This is due to MeCN exhibits no hydrogen bonding with the dye molecules (Fig. 5). In DMF solution, the two major bands appeared at 570 and 610 nm in very low concentrations. Increasing concentration from 0.05 to 0.15 mM caused a hypsochromic shift of the first absorption band (from 570 to 557 nm). After increasing concentration from 0.15 to 0.65 mM, a new main absorption band appeared at between 517 and 513 nm. This new main higher energetically electronic absorption band was attributed to the hydrazone-dimer which was prevailed at high concentration. According to this result, the intermolecular hydrogen bonding undergoes gradual stretching, and further dilution causes monomerization by rupture of this intermolecular hydrogen bonding, and its conversion is due to the intramolecular hydrogen bonding inside the monomer at very low concentrations.

The UV–vis. absorption spectra of EBB were studied in DMF solutions at different temperatures in the range of 30–70 °C (Fig. 7). The alternation in the absorption spectra showed that the absorption values of azo-hydrazone dye forms were decreased with increasing temperature. The most probable explanation is that increasing the temperature of EBB solution increased the charge delocalization, reduced the intermolecular hydrogen bonding, and consequently assisted dimer dissociation.

The monomer–dimer equilibrium can be given at below equation.

Table 4
Thermodynamic data for dimerization of EBB in DMF.

Solvent	ΔH_{dim} (kJ mol^{-1})	ΔS_{dim} (J K^{-1} mol^{-1})	ΔG_{dim} (kJ mol^{-1})	R^2
DMF	35.47	134.62	−4.67	0.990

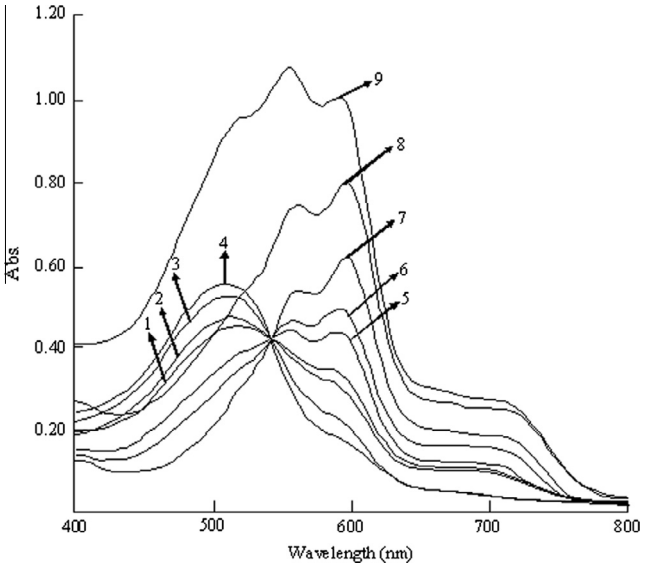

Fig. 8. Electronic absorption spectra of 0.30 mM solution of EBB in DMF–MeCN mixtures. (1) MeCN–DMF (9v/1v); (2) MeCN–DMF (8v/2v); (3) MeCN–DMF (7v/3v); (4) MeCN–DMF (6v/4v); (5) MeCN–DMF (5v/5v); (5) MeCN–DMF (4v/6v); (7) MeCN–DMF (3v/7v); (8) MeCN–DMF (2v/8v); (9) MeCN–DMF (1v/9v).

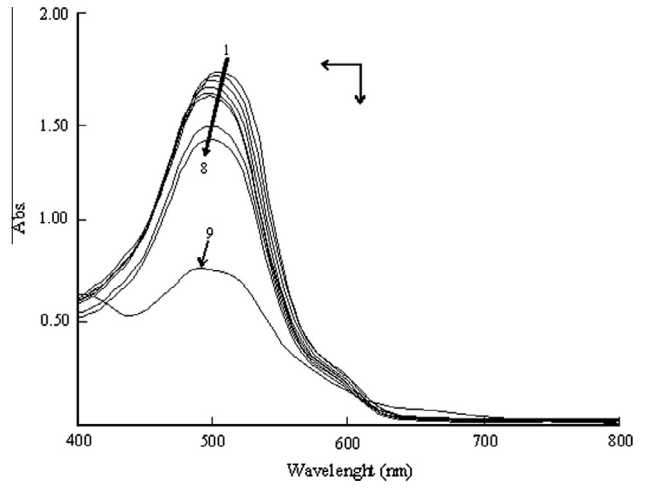

Fig. 9. The time dependent spectra of EBB in MeCN solution (c = 0.80 mM). For each curve is given the time interval in hours that is gone from the preparation of the solution up to the registration of the spectrum. 1 – 5 min, 2 – 15 min, 3 – 40 min, 4 – 1 h, 4 – 3 h, 5 – 24 h, 6 – 72 h, 7 – 168 h, 8 – 3060 h, 9 – 5760 h.

$$M + M \leftrightarrow M_2 \quad K_{dim} = \frac{[M_2]}{[M]^2} \tag{2}$$

In the above equation, M is the monomer, M_2 is the dimer and K_{dim} is the dimerization constant.

The experimental data at λ_{max} was also analyzed with Eq. (3) [34].

$$\frac{A}{c_{tot}l} = \frac{\sqrt{1+8K_{dim}c_{tot}}-1}{4K_{dim}c_{tot}}\left(\varepsilon_{mon} - \frac{\varepsilon_{dim}}{2}\right) + \frac{\varepsilon_{dim}}{2} \tag{3}$$

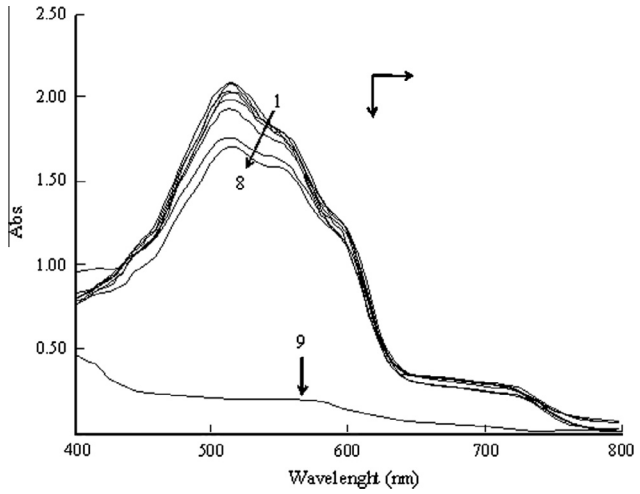

Fig. 10. The time dependent spectra of EBB in DMF solution (c = 0.70 mM). For each curve is given the time interval in hours that is gone from the preparation of the solution up to the registration of the spectrum. 1 – 5 min, 2 – 15 min, 3 – 40 min, 4 – 1 h, 4 – 3 h, 5 – 24 h, 6 – 72 h, 7 – 168 h, 8 – 3060 h, 9 – 5760 h.

In the above equation, ε_{mon} and ε_{dim} are the absorption coefficients of the monomer and the dimer.

The thermodynamic parameters for the dimerization of EBB were calculated from the experimental data by using the following equations. The values of ΔH and ΔS were determined from the slopes and intercepts of the plots of $\ln K_{dim}$ vs. $1/T$ (not shown). The thermodynamic parameters were given in Table 4.

$$\ln K_{dim} = \frac{\Delta S}{R} - \frac{\Delta H}{RT} \tag{4}$$

$$\Delta G = \Delta H - T\Delta S \tag{5}$$

The thermodynamic data showed that the driving force for dimerization of EBB was entropy. Also, the unfavorable overall enthalpy changes on dimerization indicated that repulsion between the charged sulfonate groups was the maximum. The loss of solvent order around a hydrophobic naphthol group provided the driving force for the dimerization of EBB. This result suggested that the dye–dye interactions were not the major driving force behind aggregation. It may be due to the solvent molecules formed a relatively ordered solvent cage around the hydrophobic naphthol group.

4.3.4. The effects of mixed solvents and time on the spectral absorption pattern

In order to study the H-bonded complexes between EBB molecule and DMF, the UV–visible spectra of isomolar EBB solutions were recorded in MeCN with different DMF content. As shown in Fig. 8, the spectra recorded in DMF/MeCN mixtures exhibited an isosbestic point at 545 nm indicating the equilibrium between the azo dye form and the H-bonded form of the dye. The absorbance of the monoionic hydrazone-monomer band at 574 nm and di-anionic azo form band at 598 nm increased with increasing DMF concentration in MeCN/DMF solutions (Fig. 8). This result showed that DMF molecules had a greater tendency than MeCN to form solvated complexes with the dye molecule due to the low ionization potential of DMF as well as to high H-bond-accepting character.

The effect of time on the electronic absorption spectra of EBB in MeCN and DMF solutions was studied in the period of 5760 h at 22 ± 1.0 °C in a dark area (Figs. 9 and 10). In MeCN solution, the main absorption band showed a hypsochromic shift from 508 to 496 nm with time. The electronic absorption band of EBB showed

a bathochromic shift from 514 to 532 in DMF and 525 to 550 nm in water solutions, due to the monomerization of the hydrazone dimer species of EBB.

5. Conclusions

The azo-hydrazone tautomeric equilibrium of EBB was investigated by using UV–visible absorption spectroscopy and DFT calculations. The calculated results of relative energies and mole fraction for three tautomers were showed that the azo tautomer was the only stable form of EBB in gas phase, and only one of the hydrazone tautomeric forms was found to be a lower rate (ca. 10%) in solution phase. The pH-dependence of the UV–vis. absorption spectra indicated that the EBB compound existed in acid–base, azo-hydrazone and aggregation equilibria in aqueous solution. Although, DMF and water solutions had different dielectric constants (36.71 and 78.39), azo-hydrazone tautomer formation was observed in these solutions. This behavior indicated that specific solute solvent interactions such as H-bonding and basicity effects played major role in the tautomerization and aggregation of EBB. The observed changes with increasing temperature were reversible by cooling to the initial temperature. At low concentrations, the less stable intermolecular hydrogen bonding is converted to the intramolecular hydrogen bonding.

References

[1] W.H. Ojala, E.A. Sudbeck, L.K. Lu, T.I. Richardson, R.E. Lovrien, W.B. Gleason, J. Am. Chem. Soc. 118 (1996) 2131–2142.
[2] W.H. Ojala, C.R. Ojala, W.B. Gleason, Antiviral Chem. Chemother. 6 (1995) 25–33.
[3] C. Tsopelas, R. Sutton, J. Nucl. Med. 43 (2002) 1377–1382.
[4] P.H. Rasmussen, P.S. Ramanujam, S. Hvilsted, R.H. Berg, J. Am. Chem. Soc. 121 (1999) 4738–4743.
[5] P.O. Astrand, P.S. Ramanujam, S. Hvilsted, K.L. Bak, S.P.A. Sauer, J. Am. Chem. Soc. 122 (2000) 3482–3487.
[6] F. Huang, Y. Wu, D. Gu, F. Gan, Thin Solid Films 483 (2005) 251–256.
[7] O.N. Oliveira, D.S. dos Santos, D.T. Balogh, V. Zucolotto, C.R. Mendonca, Adv. Colloid Interfaces 116 (2005) 179–192.
[8] J. Oakes, S.N. Batchelor, S. Dixon, Color. Technol. 121 (2005) 237–244.
[9] J. Oakes, P. Gratton, Color. Technol. 119 (2003) 91–99.
[10] J. Oakes, P. Gratton, Color. Technol. 119 (2003) 100–107.
[11] R. Karpicz, V. Gulbinas, A. Undzenas, J. Chin. Chem. Soc. 47 (2000) 589–595.
[12] M.A. Metwally, E. Abdel-latif, F.A. Amer, G. Kaupp, Dyes Pigments 60 (2004) 249–264.
[13] N. Menek, E. Eren, S. Topcu, Dyes Pigments 68 (2006) 205–210.
[14] M.H. Habibi, A. Hassanzadeh, A. Zeini-Isfahani, Dyes Pigments 69 (2006) 111–117.
[15] A. Hassanzadeh, A. Zeini-Isfahani, M.H. Habibi, M.R.A.P. Heravi, M. Abdollahi-Alibeik, Spectrochim. Acta A 63 (2006) 247–254.
[16] A. Priimagi, S. Cattaneo, R.H.A. Ras, S. Valkama, O. Ikkala, M. Kauranen, Chem. Mater. 17 (2005) 5798–5802.
[17] J. Oakes, S. Dixon, Color. Technol. 119 (2003) 140–149.
[18] Y.K. Zhao, W.B. Chang, Y.X. Ci, Talanta 59 (2003) 477–484.
[19] M. Rydchuk, G. Mykhalyna, O. Dobryanska, O. Korkuna, T. Vrublevska, Cent. Eur. J. Chem. 9 (2011) 886–895.
[20] N. Zaghbani, M. Dhahbi, A. Hafiane, Spectrochim. Acta A 79 (2011) 1528–1531.
[21] S. Pirillo, F.S.G. Einschlag, M.L. Ferreira, E.H. Rueda, J. Mol. Catal. B-Enzym. 66 (2010) 63–71.
[22] S. Pirillo, E.H. Rueda, M.L. Ferreira, Chem. Eng. J. 204 (2012) 65–71.
[23] M.J. Frisch, et al., Gaussian 03 Revision D.01, Gaussian Inc., Wallingford, CT, 2004.
[24] A.D. Becke, J. Chem. Phys. 98 (1993) 5648–5652.
[25] C. Lee, W. Yang, R.G. Parr, Phys. Rev. B 37 (1988) 785–789.
[26] S. Miertus, E. Scrocco, J. Tomasi, Chem. Phys. 55 (1981) 117–129.
[27] M. Cossi, N. Rega, G. Scalmani, V. Barone, J. Comput. Chem. 24 (2003) 669–681.
[28] E.S. Boes, P.R. Livotto, H. Stassen, Chem. Phys. 331 (2006) 142–158.
[29] D. Hur, A. Guven, J. Mol. Struct. (Theochem) 583 (2002) 1–18.
[30] S. Anderson, W. Clegg, H.L. Anderson, Chem. Commun. 21 (1998) 2379–2380.
[31] S.I. Gorelsky, SWizard Program, Revision 4.5., University of Ottawa, Ottawa, Canada, 2010. <http://www.sg.chem.net/>.
[32] M.M.A. Hamed, N.M. Ismail, S.A. Ibrahim, Dyes Pigments 26 (1994) 297–305.
[33] N.M. Rageh, Spectrochim. Acta A 60 (2004) 103–109.
[34] L.C. Abbot, S.N. Batchelor, J. Oakes, J.R.L. Smith, J.N. Moore, J. Phys. Chem. 108 (2004) 13726–13735.